Digital Material Fabrication Using Mask-Image-Projection-based Stereolithography

Chi Zhou, Yong Chen*, Zhigang Yang, Behrokh Khoshnevis

Daniel J. Epstein Department of Industrial and Systems Engineering
University of Southern California, Los Angeles, CA 90089, U.S.A.

*Corresponding author: yongchen@usc.edu, (213) 740-7829

Abstract

Purpose – The purpose of this paper is to present a mask-image-projection-based Stereolithography process that can combine two base materials with various concentrations and structures to produce a solid object with desired material characteristics. Stereolithography is an additive manufacturing process in which liquid photopolymer resin is cross-linked and converted to solid. The fabrication of digital material requires frequent resin changes during the building process. The process presented in this paper attempts to address the related challenges in achieving such fabrication capability.

Design/methodology/approach – A two-channel system design is presented for the multi-material mask-image-projection-based Stereolithography process. In such a design, a coated thick film and linear motions in two axes are used to reduce the separation force of a cured layer. The material cleaning approach to thoroughly remove resin residue on built surfaces is presented for the developed process. Based on a developed testbed, experimental studies were conducted to verify the effectiveness of the presented process on digital material fabrication.

Findings – The proposed two-channel system can reduce the separation force of a cured layer by an order of magnitude in the bottom-up projection system. The developed two-stage cleaning approach can effectively remove resin residue on built surfaces. Several multi-material designs have been fabricated to highlight the capability of the developed multi-material mask-image-projection-based Stereolithography process.

Research limitations/implications – A proof-of-concept testbed has been developed. Its building speed and accuracy can be further improved. Our tests were limited to the same type of liquid resins. In addition, the removal of trapped air is a challenge in the presented process.

Originality/value – This paper presents a novel and a pioneering approach towards digital material fabrication based on the Stereolithography process. This research contributes to the additive manufacturing development by significantly expanding the selection of base materials in fabricating solid objects with desired material characteristics.

Keywords: Additive manufacturing, Multi-material fabrication, Stereolithography, Digital material.

Paper type: Research paper

1. Introduction

Layer-based additive manufacturing (AM) is a collection of techniques for manufacturing solid objects by sequential delivery of energy and/or material to specified points in space to produce that solid. Differentiated from conventional manufacturing processes, a unique capability of the AM processes is that multiple materials or functionally graded material can be added in a single component during the building process. An example of such multi-material AM systems is the OBJET Connex series (*www.objet.com*). Based on its PolyJet Matrix Technology, these three-dimensional (3D) printers are capable of manufacturing complex internal structures with digital materials. That is, by combining two base materials in specific concentrations and structures, as many as 51 different materials can be created in a single printed part [1]. Hence product components can have material designs with desired mechanical properties, e.g. both soft and hard materials can be embedded in products such as tooth brushes and remote controllers. Such fabrication capability also opens up exciting new options that were previously impossible.

Our work is motivated by the recent 3D printer development especially by the digital material fabrication in which two base materials are used to define a wide variety of new materials. Note the OBJET Connex machines are based on jetting model materials from designated micro-scale inkjet printing nozzles. Such a process has inherent limitations on the selection of base materials since the jetted liquid needs to have certain viscosity and curing temperature properties in order to be jetted. We investigated the feasibility of other AM processes for the digital material fabrication to significantly expand the base material selections. Besides the inkjet printing technology, the fused deposition modeling (FDM) process can be extended for fabricating parts out of multi-materials since FDM already has separate extrusion nozzles for the build and support materials. Khalil et al. [2] presented a multi-nozzle deposition system for producing 3D tissue-engineered scaffolds. However, the FDM process has limitations on its minimum nozzle size and is relatively slow. Hence FDM is not suitable for digital material fabrication. There have also been attempts at using selective laser sintering (SLS) for multi-material fabrication [3-7]. However, accurate material feeding and recoating required by the digital material fabrication is difficult to be integrated into the SLS process.

In this research we have focused on another representative AM process, Stereolithography Apparatus (SLA). By using a laser and liquid photocurable resin, SLA offers high quality surface finish, dimensional accuracy, and a variety of material options. To address its speed limitation, we focused our research on the mask-image-projection-based Stereolithography (MIP-SL) process instead. An illustration of the MIP-SL process is shown in Figure 1. Instead of the laser used in SLA, a Digital Micromirror Device (DMD) is used in the MIP-SL process to dynamically define mask images to be projected on a resin surface area. A DMD is a microelectromechanical system (MEMS) device that enables one to simultaneously control ~1 million small mirrors to turn on or off a *pixel* each at over 5 KHz. In the MIP-SL process, the three-dimensional (3D) CAD model of an object is first sliced by a set of horizontal planes. Each thin slice is then converted into a two-dimensional (2D) mask image. The planned mask image is then sent to the DMD. Accordingly the image is projected onto a resin surface such that liquid photocurable resin can be selectively cured to form the layer of the object. By repeating the process, 3D objects can be formed on a layer-by-layer basis. Compared to the laser-based SLA, the MIP-SL process can be much faster due to its capability to simultaneously form the shape of a whole layer. Two test parts built by our prototype MIP-SL system using two different materials are also shown in the figure.

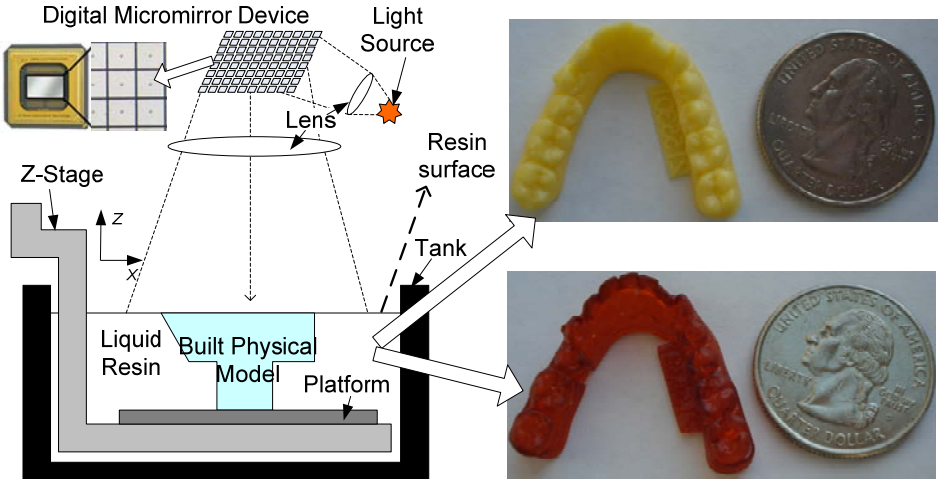

Figure 1 An illustration of the MIP-SL process

2. Principles of a Mask-Image-Projection-based SL System for Digital Material Fabrication

Multiple vats are required for different types of liquid resin in the multi-material SLA and MIP-SL processes. As a natural extension to the single material SLA system, Maruo et al. [8] first presented a multiple material stereolithogarphy system by manually removing the vat from the platform and draining

the current material, rinsing the vat, returning the vat to the platform, and dispensing a prescribed volume of a different material into the vat. However, based on the lengthy process of manually changing the materials, the system was limited to simple 2.5D microstructures. Wicker et al. [9-11] extended the work by developing a multiple vat carousel system to automate the building process including washing, curing and drying cycle between build materials. Based on similar ideas, Choi et al [12] reported a multi-material MIP-SL system for fabricating micro-scale objects. Arcaute et al. [13] and Han et al. [14] also presented an automatic material switching approach by dispensing the solution using a pipette into a custom-made small vat, and subsequently washing the current solution before changing to the next solution. Based on the technique, fabricated 3D scaffolds for heterogeneous tissue engineering have been demonstrated.

A core challenge in the use of multiple materials in SL is how to manage material contamination between changing different materials used in the fabrication process. The previous research [8-14] on developing multi-material SLA and MIP-SL systems are all based on the top-down projection. As shown in Figure 2, in order to accommodate the part size in the *Z* direction, a large tank has to be maintained for keeping the resin level. Due to the deep vat, draining and cleaning the current resin before changing to another resin vat takes a long time and leads to significant material waste. To address the problem, Kim et al. [15, 16] presented a process planning approach to minimize the material changeover number for a given multi-material CAD model. That is, if different materials are separated in a CAD model, one material can be built fully, or as much as possible, before transferring to another material. Even though the approach is able to reduce the material changeover efforts, it is not a general approach, especially for digital material fabrication, in which different materials are interlocked with each other.

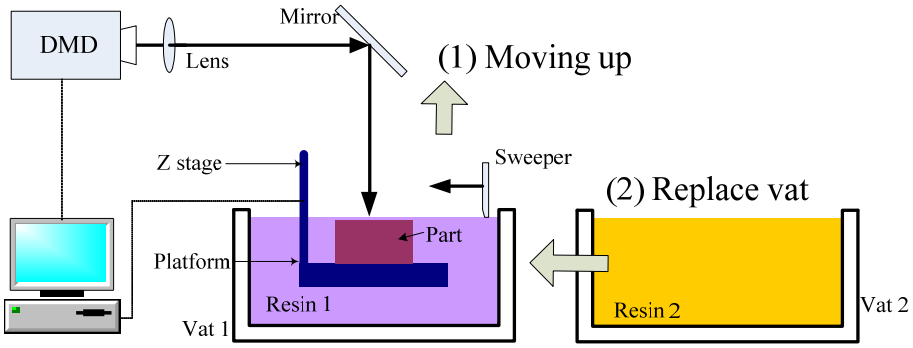

Figure 2 An illustration of the multi-material SL process based on top-down projection

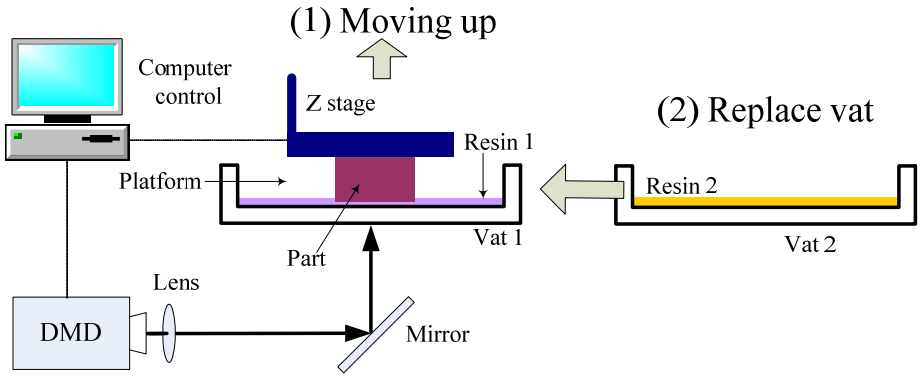

Figure 3 An illustration of the multi-material SL process based on bottom-up projection

Building functional microstructures, especially digital material fabrication, require the development of a general MIP-SL process similar to the polyjet process that can fabricate all combinations of multiple resins. The main challenge to be addressed in such a multi-material MIP-SL system is reduction of material waste and increase in cleaning efficiency during the resin tank switching process. To address the problem, we investigated the bottom-up projection in the multi-material MIP-SL process. An illustration

of such a system is shown in Figure 3. The light source is projected from the bottom of the transparent vat. Since the current built layer is formed at the bottom of the platform, the container depth is independent of the part height. Thus the liquid in the vats can potentially be as shallow as a layer thickness. When switching resin tanks, only the portion of the built model that contacts the liquid resin needs to be cleaned. Thus the material changeover efforts can be significantly reduced with less material waste.

Our efforts in developing such a bottom-up projection based MIP-SL system are presented for digital material fabrication. The remainder of the paper is organized as follows. Part separation study is presented in Section 3. An approach to reduce part separation force is presented in Section 4. Transition between multiple tanks is presented in Section 5. The experimental setup for performing physical experiments is discussed in Section 6. The experimental results of multiple test cases are presented in Section 7. Finally conclusions with future work are presented in Section 8.

3. Part Separation Study of the Bottom-up Projection based MIP-SL Process

In the bottom-up projection based MIP-SL process, a cured layer is sandwiched between the previous layer and the resin vat. The solidified material may adhere strongly to the corresponding rigid or semi-rigid transparent solidification substrate, causing the object to break or deform when the build platform moves away from the vat during the building process. One approach to conquer the attachment force is to increase the exposure to significantly over-cure the current layer such that its bonding force with the previous layer can be increased. At the same time, over-curing can lead to poor surface quality and inaccurate dimensions. Another approach to address the problem is to apply a certain coating on the resin vat such that the attachment force can be reduced. Suitable coatings, including Teflon and silicone films, can help the separation of the part from the vat [17, 18]. A coated Teflon glass has also been used in the machines of Denken [19] and EnvisionTec [20].

Even with the intermediate material, the separation force can still be relatively large. Huang and Jiang [18] investigated the attachment force for the coating of an elastic silicone film. Based on a developed on-line force monitoring system, test results indicate that the pulling force increases linearly with the size of the working area. Experiments indicate that, for a square of 60×60mm, the pulling force to separate the part from the film is greater than 60 N. Such a large attachment force between the cured layer and the vat is a key challenge to be addressed in the development of the bottom-up projection based MIP-SL system.

In our research, another type of coating material, Polydimethylsiloxane (PDMS, Sylgard 184, Dow Corning), is applied on the resin vat. This selection is based on a unique property of the PDMS film during the polymerization process that was identified in [21]. Dendukuri *et al* [21] presented a photolithography-based microfluidic technique for continuously fabricating polymeric particles. The developed technique is based on the oxygen-aided inhibition near the PDMS surfaces to form chain-terminating peroxide radicals. In the process a very thin oxygen inhibition layer (~2.5 μm) is formed that can prevent the cured layer from attaching to the PDMS film. We studied the part separation forces based on the PDMS film. The experimental results are discussed as follows.

3.1 Separation Forces for Solidified Resin based on the PDMS Film

A set of physical experiments have been performed to investigate the separation force of a cured layer based on a coated PDMS glass. The setup for measuring the pulling force is shown in Figure 4.a. Two FlexiForce sensors (Tekscan, South Boston, MA) with a range of 0-25 lbs are sandwiched between the fixture and vat. Since the vat is free at the bottom and the side, and only fixed at the top, the pulling force by the part will be transferred to the sensors when the platform rises. The two sensors are connected to a microcontroller, which can sample and record the sensors' readouts at over 3KHz. In the experiments, we first use a given mask image to build a certain number of layers (e.g. 25 layers). We then begin to record the separation force in the building process of the next few layers. For each layer, after the designed mask image has been exposed for a certain time, the platform is raised up slowly at 0.6mm/sec and the related readouts of the two sensors are then recorded.

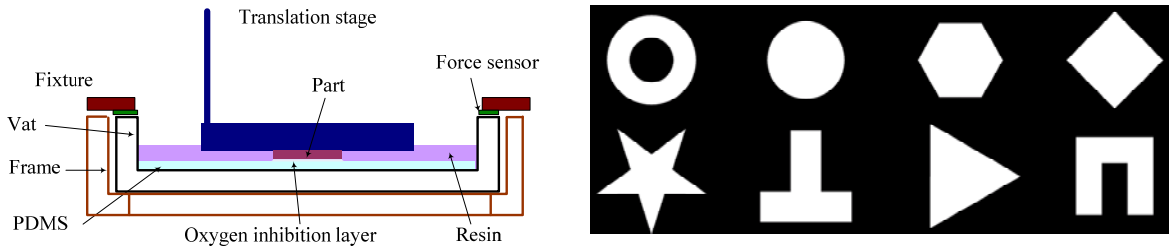

(a) One channel system with PDMS film (b) Different projection patterns with the same area

Figure 4 Experimental setup for studying part separation forces in the MIP-SL process

The three factors potentially affecting the separation force that were considered in our study include (1) exposure time, (2) image area, and (3) image shape. To understand the effects of these factors, designed experiments were conducted. Figure 4.b shows a set of mask images that have been used in the experiments for testing the effect of image shapes. The tested projection patterns, including triangle, square, hexagon, circle, t-shape, u-shape, band, and star-shape, have the same area in each test. Figure 5 shows the measured separation forces of a sensor for different test cases. The horizontal axis indicates the distance in the *Z* direction (in the unit of 10 μm), and the vertical axis indicates the recorded pulling force (in ounces).

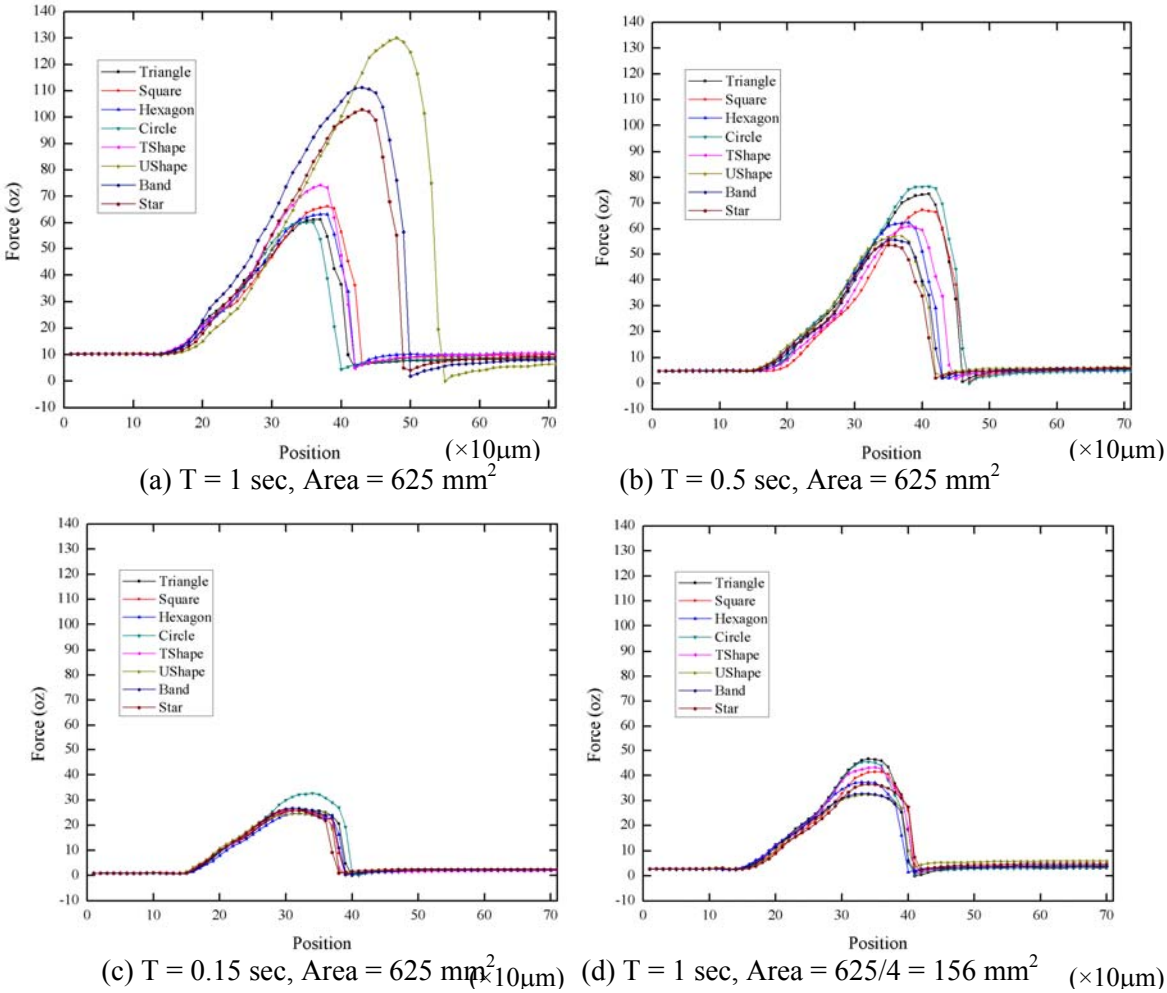

(a) T = 1 sec, Area = 625 mm^2 (b) T = 0.5 sec, Area = 625 mm^2

(c) T = 0.15 sec, Area = 625 mm^2 (d) T = 1 sec, Area = 625/4 = 156 mm^2

Figure 5 Pulling forces of cured layer from a PDMS film in different test cases

Based on the experimental results, it can be observed that:

(1) As the *Z* stage moves up, the separation force increases until it reaches a peak value when the cured layer is detached from the PDMS film;
(2) The peak force gets larger when the same mask image is exposed longer;
(3) The peak force gets larger when a larger image area is projected;
(4) The image shape has more complex effects on the peak force. In addition, their effects may interact with the exposure time and the projection area;
(5) With the coated PDMS film on the vat, the separation force is still considerably large (~100 oz or 27.8 N for an image area of 625mm^2 with 1 second exposure).

3.2 Separation Force for Liquid Resin without Curing

A similar set of experiments was conducted to analyze the pulling force of a part without liquid resin being cured between the part and the vat. In the experiments, we first used an image of a square (35mm×35mm) to build a certain number of layers (e.g. 25 layers). The built part was then lowered to form a certain gap with the PDMS film. Without exposing any image to cure liquid resin, the platform was then raised up slowly at 1.2mm/sec and the related separation forces were recorded on the force sensors. Different gap sizes (0.1- 0.5mm) were tested. The experiment result is shown in Figure 6. It can be seen that:

(1) The separation force is smaller than the related cases with solidified resin;
(2) The separation force decreases with a larger gap size between the part and the PDMS film;
(3) The separation force can only be neglected until the gap size is larger than 0.5 mm.

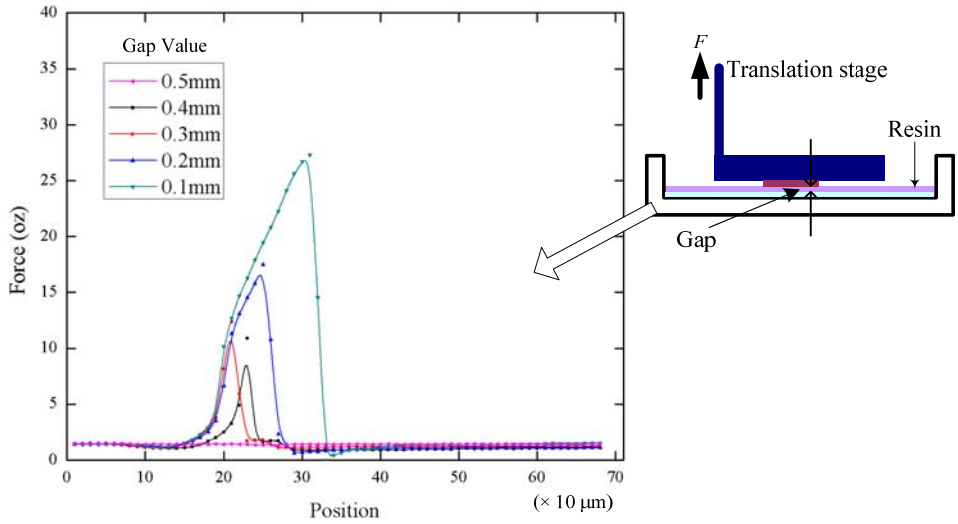

Figure 6 Pulling forces of a built part from a PDMS film for different gap sizes

4. Two-Channel Design for the Bottom-up Projection based MIP-SL Process

The large separation force between the cured layer and the resin vat may fail the building process when the bonding force between the current layer and previous layers is smaller than the separation force. In addition, the PDMS film will have cracks after building multiple layers due to the cyclic loading and the related material fatigue.

To facilitate the bottom-up projection based MIP-SL process, a new two-channel design has been developed, which can fundamentally address the large separation force in the building process. The developed approach is motivated by the following two observations:

(1) As discussed in [18], after the resin is sufficiently cured, there is a large suction force between the cured layer and the silicone film. Hence the maximum pulling force as shown in Figure 5 is related to the release of the cured layer from the film.

(2) As demonstrated in [21], the oxygen-aided inhibition around the PDMS surface leaves a non-polymerized lubricating layer near the PDMS film. Consequently the cured layer can easily slide on the PDMS surface.

Figure 7 shows an illustration of the developed two-channel system design. In our method, a transparent PDMS film is applied on half of the bottom surface of a transparent glass vat. Hence the resin vat is divided into two channels, with and without the PDMS film. A mask image is exposed only on the channel with PDMS. As shown in Figure 7, after a layer is cured at Position (1), the vat is moved along the *X* axis such that the part is moved to the channel without PDMS (i.e. Position 2). Hence the large suction force between the cured layer and the PDMS film would be avoided. If the PDMS film is thick enough (e.g. >0.5mm), the part would be easily separated from the vat. After moving the part up by a certain distance *d* (position 3), the vat is moved back such that the part is on top of the channel with PDMS (position 4). Finally the platform moves down by a distance (*d – layer_thickness*) for the building of a new layer. Note that the motion in the *X* direction is by the vat and the related frame. Hence the accuracy of the MIP-SL system is not affected by the *X* translation since there is no relative motion between the platform and the projection device.

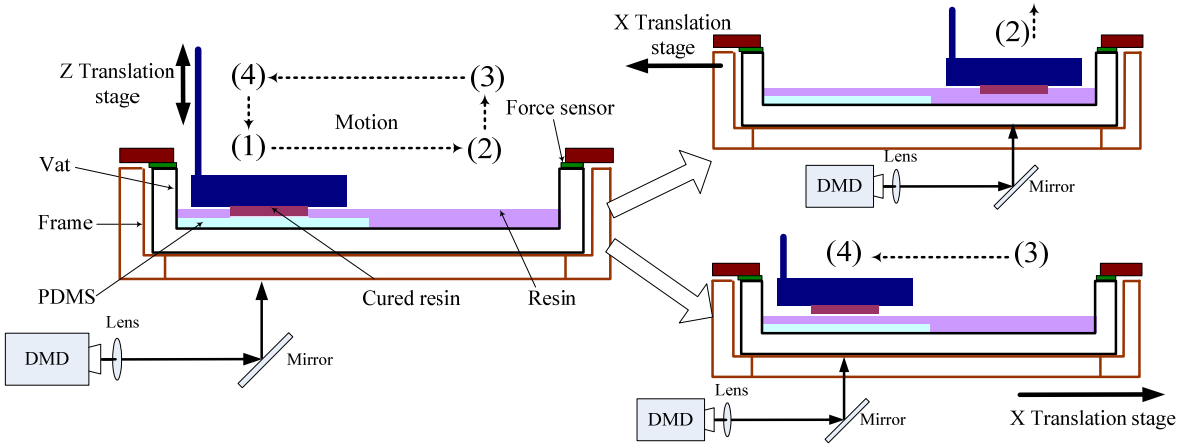

Figure 7 Two-channel system with PDMS

An appropriate thickness of the coated PDMS film can be determined by considering the following factors:

(1) The thickness of the oxygen inhibition layer (around 2.5μm) on the PDMS surface is independent of the thickness of the PDMS film [21]. Thus the exerted force in the *X* direction is not directly related to the PDMS film thickness.

(2) More light energy will be taken away by the film if the PDMS film is thicker;

(3) The PDMS film should be thick enough such that the gap between the cured layer and the vat surface at Position (2) will be large enough to have a small separation force.

(4) More resin has to be maintained for a thicker PDMS film in the channel without PDMS.

Considering all the above factors, in our prototype system the PDMS film thickness is set at 1mm. The separation and shearing forces of the related two-channel design are discussed as follows.

4.1 Separation Forces for Solidified Resin

To verify the proposed two-channel system design, physical experiments that are similar to the ones in Section 3.1 have been conducted. The same setup as shown in Figure 4.a has been used in measuring the separation forces. The same mask images as shown in Figure 4.b have been used in building test layers. The same experiments as described in Section 3.1 for the two-channel system design were repeated. The test results are shown in Figure 8. In each figure the curves record both the sliding and pulling-up stages. The figures show that the force in the *Z* direction is very small when sliding the resin vat. During the platform pulling-up stage, the peak separation forces are also relatively small (around 2-4 oz or ~0.83 N). The measured forces are only 4-5% of the related measured forces observed in the single channel design.

In addition, the variations of the exposure time, the image area and the image shape have smaller effects on separation forces in the new design.

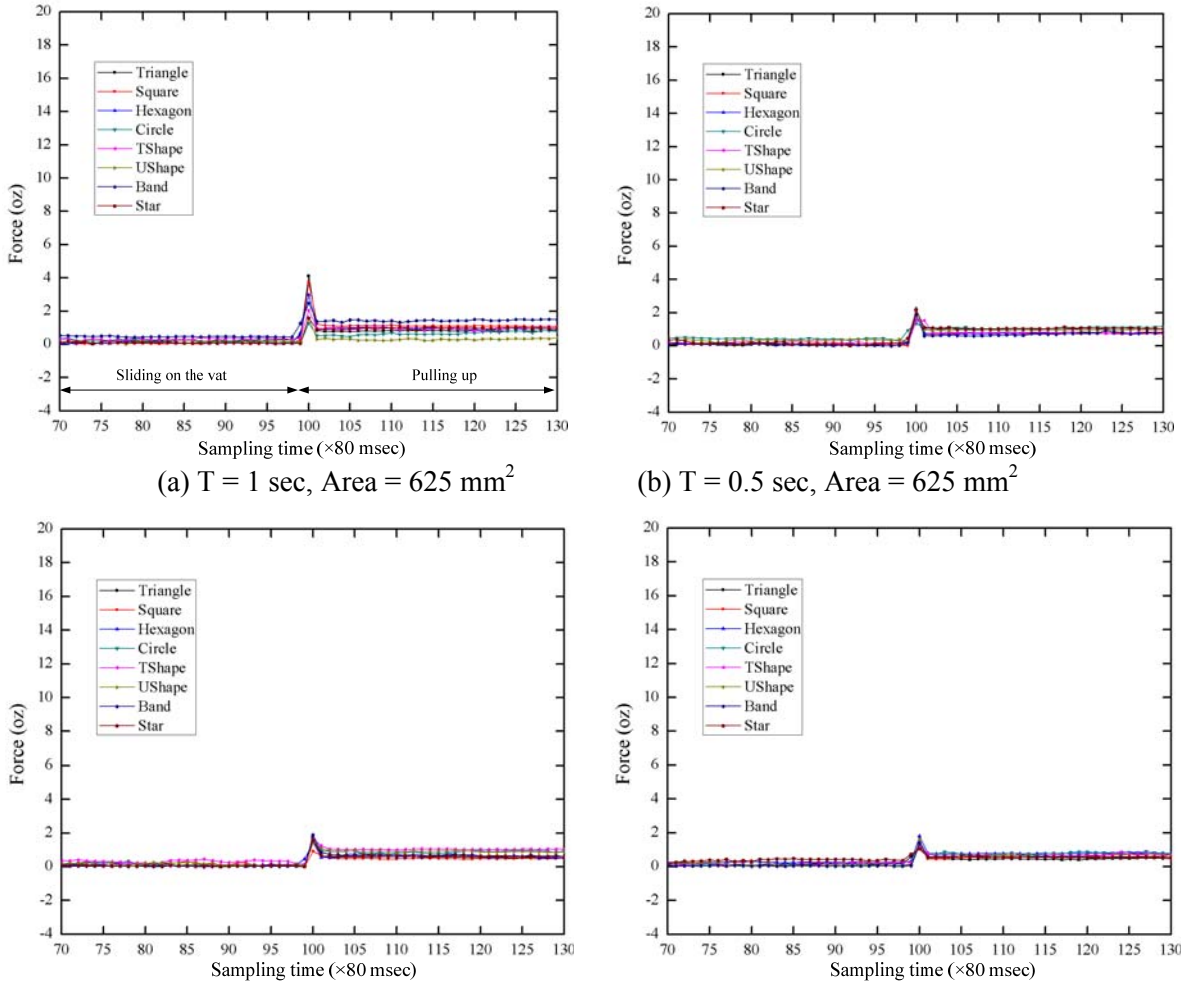

(a) T = 1 sec, Area = 625 mm^2 (b) T = 0.5 sec, Area = 625 mm^2

(c) T = 0.15 sec, Area = 625 mm^2 (d) T = 1 sec, Area = 625/4 = 156 mm^2

Figure 8 Pulling forces of cured layer for two-channel system in different test cases

4.2 Shearing Forces in the *X* Direction

The FlexiForce sensors were used in a modified setup to measure the shearing force in the *X* direction. However, no meaningful readouts were recorded from the sensors due to the small shearing force. To quantitatively estimate the value of the shearing force, a set of square rods with different sizes was built using the two-channel system. The built rods shown in Figure 9 are 10mm tall. The minimum cross section size is 0.3×0.3mm. Note that we also successfully built rods with even smaller sizes. However, the rods were so fragile that they lost the mechanical strength to sustain themselves when the part was taken out of the resin vat and washed in isopropyl alcohol.

For a rod with a cross section size of 0.3×0.3mm, the upper bound on the tangential force that can be applied on it can be analytically estimated. As shown in Figure 9, the testing rods in the experiment can be modeled as a cantilever beam. Suppose the length of the beam is *L*, the size of the beam section is *b***b*, and the force in the tangent direction is *F*. The maximum bending stress occurs at the end and can be calculated as: $\sigma = Mc/I$, where $M = L \times F$, I is the section modulus, $I = b^4/12$, and $c = b/2$. Put them together, we have $\sigma = \frac{6FL}{b^3}$. Suppose the allowable bending stress is $[\sigma]$ and the minimal beam section

size is $[b]$. We will have the following equation: $F \le \frac{[\sigma][b]^3}{6L}$. The parameters for this experiment are listed as follows: $[\sigma]$=65MPa, $[b]$=0.3mm, and L=10mm. According to the equation, the upper bound of the tangential force is only 0.03N or 0.11oz. Compared to the separation force in the Z direction, the shearing force in the X direction is rather small.

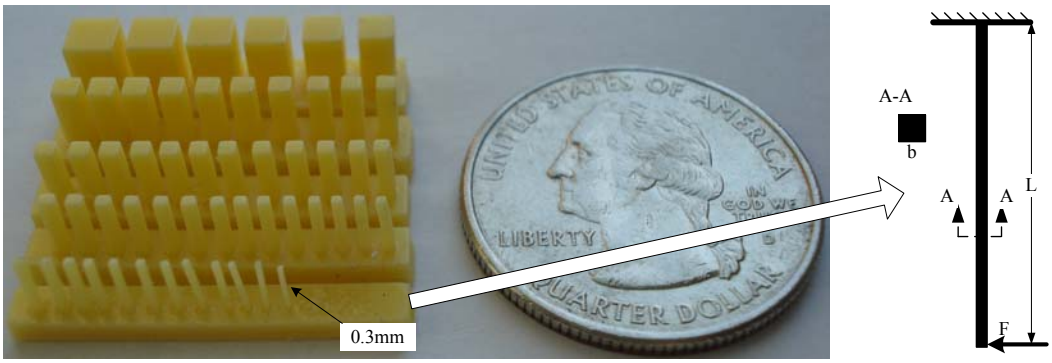

Figure 9 Shearing force verification test

5. Transition between Multiple Tanks

As discussed before, the challenge of using multiple materials in the MIP-SL process is managing the contamination between different materials. The proposed two-channel system leads to a smaller separation force in the bottom-up projection. Hence shallow vats can be used in the MIP-SL process to reduce the material waste and the required cleaning effort. To ensure no contamination between different resin vats, different cleaning strategies have also been explored and identified.

5.1 Shallow Vat Study

It is desired to have as little liquid as possible in a resin vat to reduce the contact of the part and liquid resin. However, when the thickness of liquid resin in a tank is too small, islands that have no liquid will appear on the bottom surface due to liquid surface tension. Hence the minimum thickness of liquid resin on the PDMS surface needs to be determined based on the tested resins. A scaled syringe was used to gradually inject resin into the two-channel tank until the resin can fully cover the whole PDMS surface. As shown in Figure 10, the related thickness for Perfactory SI500 (yellow color) resin is found to be ~0.5mm. Reducing the viscosity of resin can reduce the surface tension and accordingly the minimum resin thickness. During the building process, a pump can be used to dynamically add liquid resin into the vat to compensate for the material consumption.

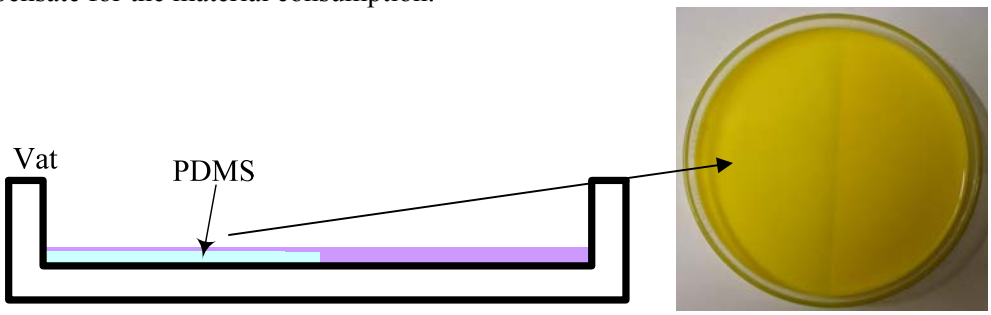

Figure 10 Minimum thickness of resin on the PDMS surface

5.2 Cleaning Resin Residue on Built Layers

Liquid resin may accumulate around the perimeter of the object and at the bottom of the cured layer when it is raised from the vat. To avoid material contamination when changing resin vats, the excessive materials on the bottom and the side of part surface should be removed before building a new layer.

Various cleaning approaches have been tested. The best candidate we identified is a two-stage cleaning strategy based on:

(1) ***Rough cleaning***: a soft brush is moved relative to the part, which can remove the majority of liquid resin on the bottom and the perimeter of the part. The resin collected in the brush tank can be recycled to refill the building tank.

(2) ***Final cleaning***: Due to the surface tension, resin residue can still be found on the part surface after the rough cleaning. To thoroughly clean the resin residue, ultrasound cleaning was identified as the most effective approach for final cleaning. After immersing the bottom portion of the built part in a liquid solvent (e.g. 90% isopropyl alcohol and 10% water by volume), high frequency ultrasound vibration is provided. The applied ultrasound will form microscopic bubbles on the part surface, which will then implode under the pressure of agitation. The generated shock waves will impinge on the part surface. Consequently the resin can be quickly and thoroughly rinsed in all directions. The approach is especially effective for resin inside small cavities, which is difficult to remove using other cleaning methods.

After final cleaning, the part is wetted with solvent. It must be dried before being immersed into another material; otherwise, a new layer cannot properly adhere to the previous layer. In our prototype system a fan is used to blow dry air on the part to dry out the alcohol residual. After the part is dry, the building process may resume and layers of a different material can be added.

For two types of materials (*A* and *B*), the required stations in our prototype system consist of two resin vats, two brush tanks, an ultrasound cleaner, and a fan (refer to Figure 11.a). Even though the shallow vat requires only a small amount of material to be cleaned in the system, the cleaning procedure takes the majority of the cycle time, which significantly reduces the throughput of the whole process. Hence, reducing the number of material alternations is important in the multi-material MIP-SL system.

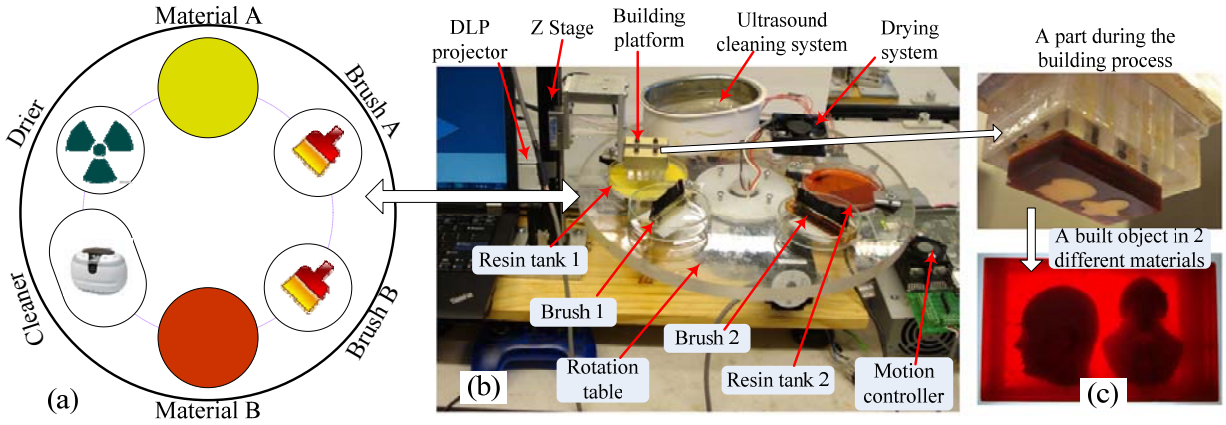

Figure 11 Hardware system of the prototype multi-material MIP-SL system

6. Experimental Setup

6.1 Hardware System

A prototype system has been built for verifying the presented methods. The hardware setup of the developed multi-material MIP-SL system is shown in Figure 11.b. In the designed system an off-the-shelf projector (*CASIO XJ-S36*) was used. The use of a commercial projector can significantly reduce the prototype cost and simplify the system design. The optical lenses of the projector were modified to reduce the projection distance. Various projection settings including focus, key stone rectification, brightness and contrast were adjusted to achieve a sharp projection image on the designed projection plane. The DMD resolution in our system is 1024×768 and the envelope size is set at 48×36 mm. A linear stage from VELMEX Inc (Bloomfield, NY) is used as the elevator for driving the platform in the *Z* axis. A rotary table also from VELMEX Inc is used to rotate the resin vats and cleaning stations. A high performance 4-

axis motion control board with 28 Bi-directional I/O pins from Dynomotion Inc. (Calabasas, CA) is used for driving the linear stages and controlling the ultrasound cleaner, the fan, and a shutter. Two flat and clear glass Petri dishes are used as resin tanks. A PDMS film (Sylgard 184, Dow Corning) is coated on each glass dish. Figure 11.c shows the building of a test part in two materials.

6.2 Software System

Figure 12 shows the flowchart of the multi-material MIP-SL process. Note that the part will only be cleaned during the transitions between building layers in different materials. If the same material is used in a single layer or two neighboring layers, then no cleaning is performed. We also alternate the building sequence of two materials in neighboring layers (i.e. $A_i \rightarrow B_i \rightarrow B_{i+1} \rightarrow A_{i+1} \rightarrow \ldots$) such that less material switchover will be needed. A related multi-material MIP-SL software system has been developed using the C++ programming language with Microsoft Visual C++ compiler. The graphical user interface (GUI) of the developed software system is shown in Figure 12. The software system can synchronize the image projection and motion control based on geometry processing.

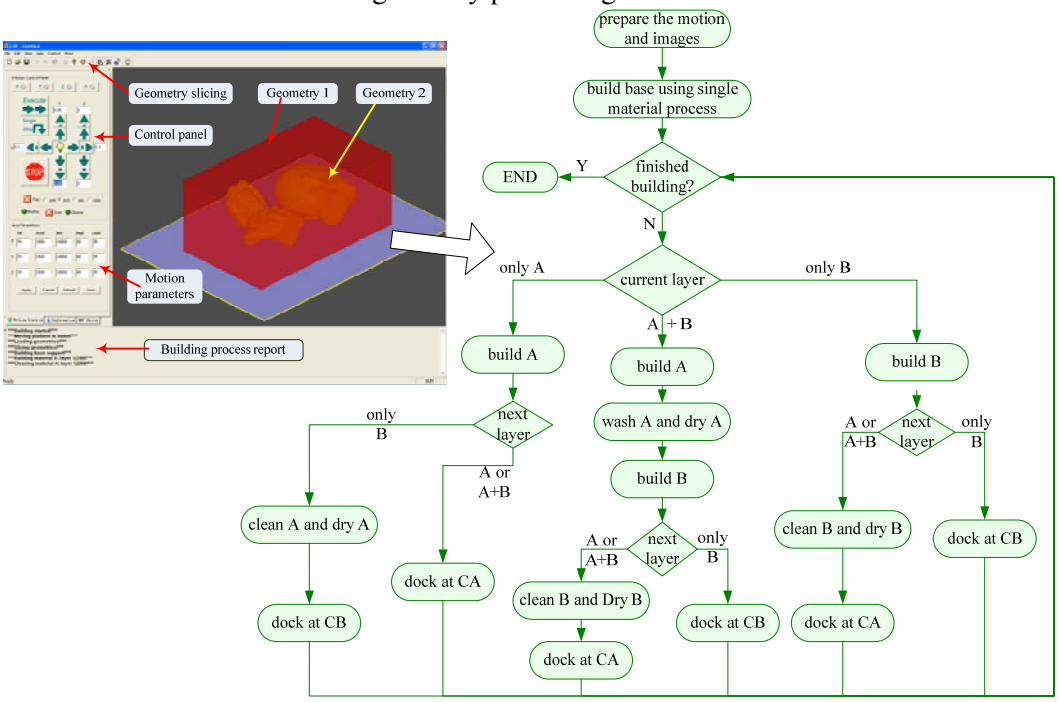

Figure 12 Flow chart of the multi-materials MIP-SL system and related software system

6.3 Materials

To test the multi-material MIP-SL system, we used Perfatory™ SI500 (yellow) and Perfactory™ Acryl R5 (red) from EnvisionTec Inc. (Ferndale, MI), FTI-GN (white) from 3D Systems Inc. (Rock Hill, SC), and a transparent resin developed inhouse. All the tested resins can be cured by blue light with a wavelength around 410nm. For the curing depth set at 0.1mm, the exposure time based on our projection system is set as 400 ms, 350 ms, 250 ms, and 300 ms for Perfatory™ SI500, Perfactory™ Acryl R5, FTI-GN white and transparent resins, respectively. Investigation of the bonding strength between the four different materials demonstrates that they can be bonded quite well due to the strong affinity between them.

7. Results and Discussion

A set of test cases has been designed to verify the developed prototype system of fabricating objects with different combinations of multiple materials. The experimental results have demonstrated that the

presented two-channel bottom-up projection based approach can successfully build parts with desired material distributions. Although the developed prototype system can only use up to two different materials, the method can be extended in a straight forward manner to fabricate objects with three or more materials.

7.1 Components with a Single Material

Various test cases based on a single material has been built using the developed prototype system. The building process is shown in Figure 12 with only one material (i.e. *A* or *B*). Without changing resin tanks, the building speed of the process for a single material is rather fast (~15 second per layer). Figure 13 shows some of the built objects based on the experimental system. The part quality was analyzed to be satisfactory.

Figure 13 Test cases for building objects in a single material

7.2 Components with Two Different Materials

A main purpose of using multiple materials in a component is to provide additional functionality in the built part, such as varying colors, electrical conductivity, or mechanical properties.

Verification of building objects with different colors: A test case based on the famous symbol of bagua is used to verify the bonding between two different materials (yellow and red resins) and to demonstrate the capability of the prototype system in building objects with different colors. The designed CAD model is shown in Figure 14.a. Accordingly the built object is shown in Figure 14.b.

Verification of building objects with different electrical conductivities: Although most Acrylate or Epoxy resins are electrically insulating, with proper modification a resin can become conductive (for example silver-filled epoxies). Embedding electrical circuits inside a 3D part is very meaningful for electrical and electronic design. In this way, a circuit with different shapes and different orientations can be achieved (e.g. 3D circuit). In addition, the circuit can be designed to be adaptive to the target object shape (e.g. curved surfaces). A designed test case is shown in Figure 15. Masks *A* and *B* are the projection image for the conductive and insulative materials, respectively (red and transparent resins). The built part is also shown in the figure, which verifies that the proposed method can be successfully used in the application.

(a) CAD model (b) Built part

Figure 14 A test case for building an object with different colors

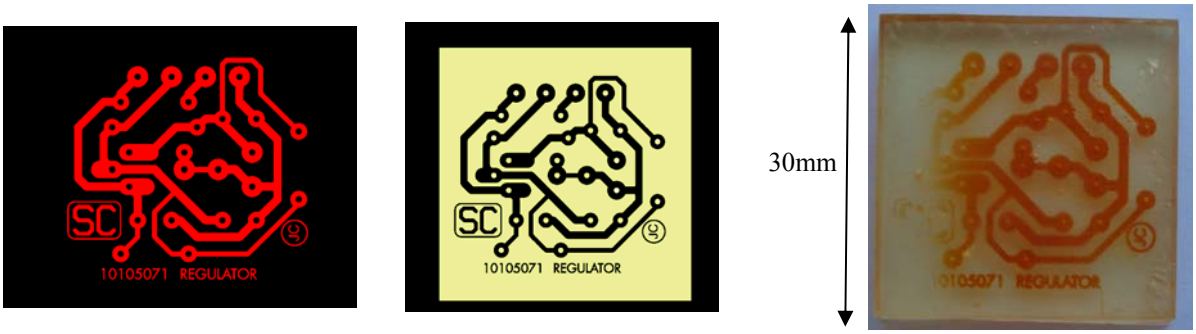

Mask *A* Mask *B* Built part

Figure 15 A test case for building an object with different electrical conductivities

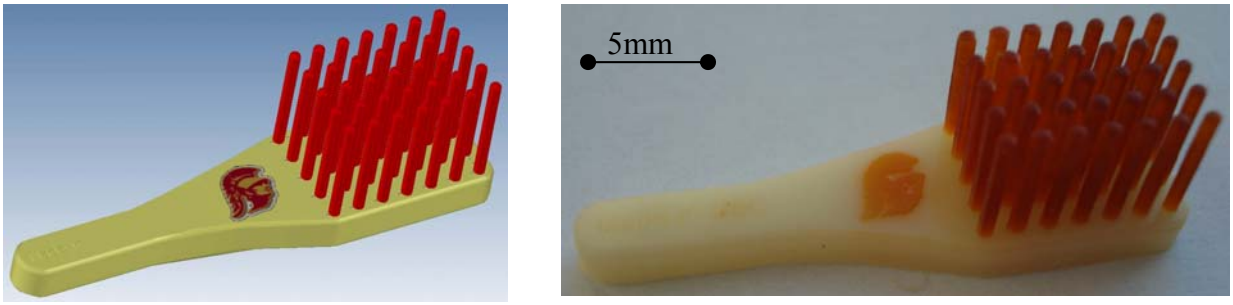

(a) CAD model (b) Built part

Figure 16 A test case for building an object with different mechanical properties

Verification of building objects with different mechanical properties: Another typical application of using multiple materials is in improving the mechanical properties of designed components. For example, some portions of a product component may be soft while others may be rigid. For this purpose, a designed test case is shown in Figure 16.a. The brush is composed of two portions: the base and the brush-head. These portions have different flexibility requirements, i.e. the base needs to be rigid while the brush-head needs to be soft and flexible. Two different materials (white and red resins) that have different mechanical properties are used in building the designed brush. The built object is shown in Figure 16.b. In addition, a USC's Trojans logo with red material is embedded inside the white base. Based on the built part, we verified that the mechanical performances of the base and the brush-head are different.

7.3 Components with Digital Materials

As demonstrated by the OBJET Connex family, the most unique feature of digital materials is that two base materials can be combined in specific concentrations and structures. Therefore product components

can have desired properties that may be different from those of the base materials. Accordingly, a designed test case is shown in Figure 17. A four grid slab with four different combinations of two materials (red and yellow resins) is shown. The ratios of the two materials are 100% vs. 0%, 75% vs. 25%, 25% vs. 75%, and 0% vs. 100%, respectively. Using a halftoning method called dithering [22], we can get different combinations of two materials by applying different dithering matrix. The built objects are also shown in the figure. The results demonstrate that our prototype system can mix two materials in predefined proportions to produce isotropic materials with different material properties.

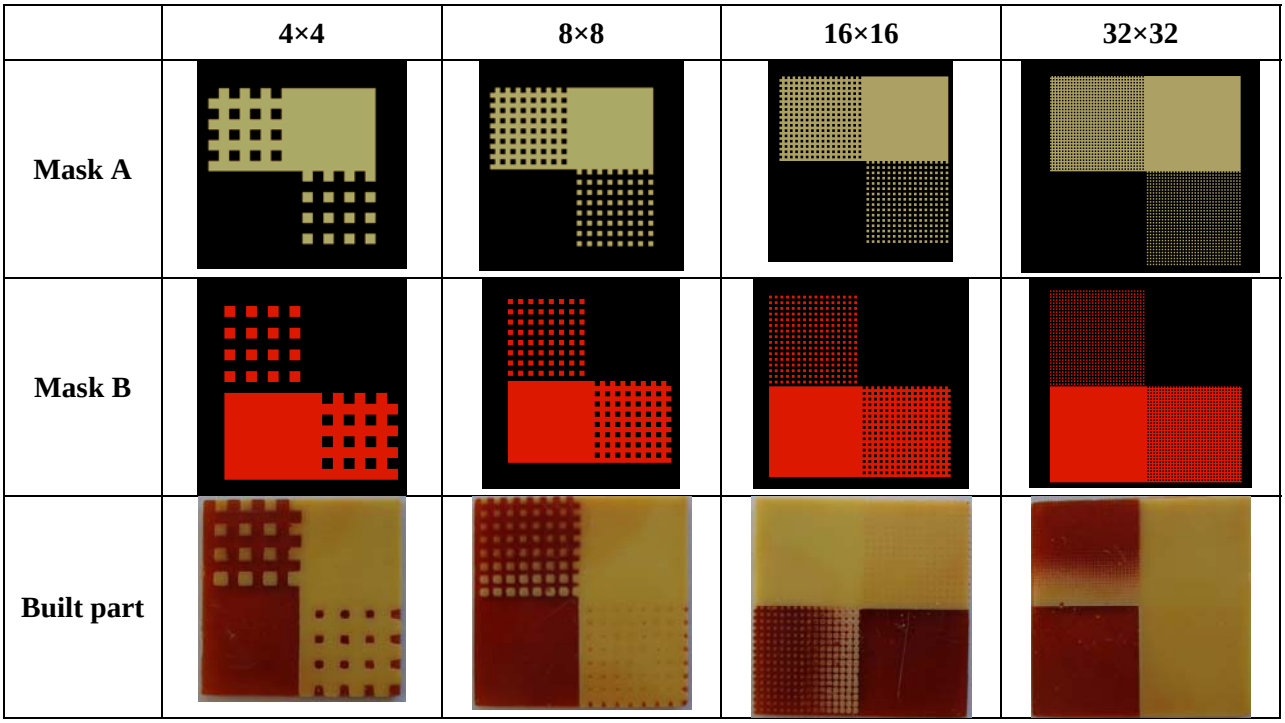

Figure 17 A test case for building an object with digital materials

7.4 Limitations and Challenges

We have presented a multi-material MIP-SL system for fabricating 3D components with spatially controlled digital materials. Multiple test cases have been performed to verify the presented approach. In our tests, several issues and potential challenges have also been identified that need to be addressed in future work:

- **Building speed:** It takes ~3 minutes for the prototype system to finish the rough and final cleaning and drying. Such cleaning procedures take the majority of the cycle time. Better hardware design and new cleaning strategy may be explored to improve the building speed.
- **Material Waste**: Even with the shallow vat design in our prototype system, we estimate that there is still ~30% material waste due to the cleaning procedure.
- **Material Bonding:** The materials we tested all belong to the same type of resins. We have not tested the bonding between different types of resins (e.g. Acrylate resins and conductive polymers). The bonding strength between different types of materials may be an issue for future development of the multi-material MIP-SL process.
- **Trapped air and bubbles:** It is noticed that, for some types of geometries (e.g. holes and cavities), there are small bubbles in the built part. This is due to the trapped air in such geometries, which needs to be addressed in future research.

- **Accuracy and resolution**: To build digital materials, it is critical to accurately control the cured shapes with high resolution; otherwise the desired material combination ratio will not be achieved. Techniques such as optimized mask image planning [23] can be used to improve the accuracy and resolution of cured shapes.

8. Conclusions

A novel mask-image-projection-based stereolithography process has been presented for fabricating objects with digital materials. The proposed approach is based on projecting mask images bottom-up. Hence a very shallow vat can be used in the building process. A new two-channel system design has been presented, which significantly reduces the separation force between a cured layer and the resin vat. A two-stage cleaning strategy has been developed to avoid contamination during the changed resin vats. The fabrication results demonstrate that the developed dual-material MIP-SL system can successfully produce 3D objects with spatial control over placement of both material and structure. The approach is general and can be easily extended from dual materials to multiple materials.

The concept of digital materials as demonstrated by the polyjet process is interesting and significant. Our work illustrates that such a concept can also be achieved by other additive manufacturing processes, thereby allowing more material choices. Combining multiple materials with various concentrations and structures to achieve desired characteristics such as multiple mechanical, electrical, chemical, biological, and optical properties can have numerous future applications. The development of 3D multi-material printers is therefore critical for future additive manufacturing research.

References

1. Digital materials: http://www.objet.com/3D-Printing-Materials/Overview/Digital_Materials/, visited on Sept/1/2011.
2. Khalil, S., Nam, J., Sun, W. (2005). "Multi-nozzle deposition for construction of 3D biopolymer tissue scaffolds". Rapid Prototyping Journal, Vol. 11 (1), pp. 9–17.
3. Jackson, B., Wood, K., Beaman, J.J. (2000). "Discrete multi-material selective laser sintering: development for an application in complex sand casting core arrays". In: Proceedings of Solid Freeform Fabrication Symposium, The University of Texas at Austin, Austin, TX, pp. 176–182.
4. Liew, C.L., Leong, K.F., Chua, C.K., Du, Z. (2001). "Dual material rapid prototyping tech- niques for the development of biomedical devices. Part I. Space creation". Int. J. Adv. Manuf. Technol., Vol. 18 (10), pp. 717–723.
5. Liew, C.L., Leong, K.F., Chua, C.K., Du, Z. (2002). "Dual material rapid prototyping tech- niques for the development of biomedical devices. Part II. Secondary powder deposition". Int. J. Adv. Manuf. Technol. Vol. 19 (9), pp. 679–687.
6. Santosa, J., Jing, D., Das, S. (2002). "Experimental and numerical study on the flow of fine powders from small-scale hoppers applied to SLS multi-material deposition". In: Proceedings of Solid Freeform Fabrication Symposium, The University of Texas at Austin, Austin, TX, pp. 620–627.
7. Regenfuss, P., Streek, A., Hartwig, L., Klötzer, S., Brabant, Th., Horn, M., Ebert, R., Exner, H. (2007). "Principles of laser micro sintering". Rapid Prototyping Journal. Vol. 13 (4), pp. 204–212.
8. Maruo, S., Ikuta, K., and Ninagawa, T. (2001). "Multi-polymer microstereolithography for hybrid opto-MEMS", Proceedings of the 14th IEEE International Conference on Micro Electro Mechanical Systems (MEMS 2001), pp. 151–154.
9. Wicker, R., Medina, F., and Elkins, C. (2005). "Multiplematerialmicro-fabrication: extending stereo lithography to tissue engineering and other novel application". In: Proceedings of Annual Solid Freeform fabrication Symposium, Austin, TX, pp. 754–764.
10. Choi, J., Kim, E. H., and Wicker, R. (2011). "Multiple-material stereolithography", Journal of Materials Processing Technology, Vol. 211/3, pp. 318-328.

11. Wicker, R., Medina,F., and Elkins, C. (2009). “Multi-material stereolithography”. U.S. Patent 7,556,490.
12. Choi, J.W., MacDonald, E., Wicker, R. (2010). “Multi-material microstereolithography”. Int. J. Adv. Manuf. Technol. Vol. 49, pp. 543–551.
13. Arcaute, K., Zuverza, N., Mann, B., and Wicker, R. (2006). “Developmentof an automated multiple material stereolithography machine”. In:Proceedings of Annual Solid Freeform Fabrication Symposium, Austin, TX, pp. 624–635.
14. Han, L., Suri, S., Schmidt, C. E., and Chen, S. (2010). “Fabrication of three-dimensional scaffolds for heterogeneous tissue engineering", Biomed Microdevices, 12, 721-725.
15. Kim, H., Choi, J., and Wicker, R. (2010). “Process planning and scheduling for multiple material stereolithography”. Rapid Prototyping J. Vol. 16, No. 4, pp. 232–240.
16. Kim, H., Choi, J., MacDonald, E., and Wicker, R. (2010). “Slice overlap detection algorithm for the process planning of multiple material stereolithography apparatus”. Int. J. Adv. Manuf. Technol. Vol. 46, No. 9, pp. 1161–1170.
17. Chen. Y., Zhou, C., and Lao, J. (2011). “A layerless additive manufacturing process based on CNC accumulation.” Rapid Prototyping Journal, Vol. 17, No. 3, pp. 218-227.
18. Huang, Y.M., Jiang, C.P. (2005). "On-line force monitoring of platform ascending rapid prototyping system", *Journal of Materials Processing Technology*, Vol. 159 pp.257-64.
19. SLP-4000 Solid Laser Diode Plotter, Product Brochure, Denken Corporation, Japan, 1997.
20. EnvisionTEC ULTRA, www.envisiontec.de/index.php?id=108, visited on Sept/1/2011.
21. Dendukuri, D., Pregibon, D. C., Collins, J., Hatton, T. A., and Doyle, P. S. (2006). “Continuous-flow lithography for high-throughput microparticle synthesis”. Nature Mater., Vol. 5, pp. 365–369.
22. Lieberman, D. and J. P. Allebach (1997). "Efficient model based halftoning using direct binary search," in Proc. 1997 IEEE Int. Conf. Image Processing, Santa Barbara, CA.
23. Zhou, C. Chen, Y., Waltz, R. A. (2009), “Optimized mask image projection for solid freeform fabrication.” ASME Journal of Manufacturing Science and Engineering, Vol. 131, No. 6, pp. 061004-1~12, 2009.